ISSN 0036-0236, Russian Journal of Inorganic Chemistry, 2024. © Pleiades Publishing, Ltd., 2024.

PHYSICOCHEMICAL ANALYSIS OF INORGANIC SYSTEMS

Phase Tree, Analysis of Crystallizing Phases, and Description of Chemical Interaction in the Ca,Ba‖F,Cl Three-Component Reciprocal System

T. D. Slavnov[a], E. M. Egorova[a], *, I. K. Garkushin[a], A. V. Burchakov[a], and M. A. Demina[a]

[a] *Samara State Technical University, Samara, 443100 Russia*

**e-mail: dvoryanova_kat@mail.ru*

Received May 19, 2023; revised August 25, 2023; accepted August 29, 2023

Abstract—The paper analyzes the phases crystallizing in the Ca,Ba‖F,Cl, ternary reciprocal system and describes ion-exchange and complexation reactions therein. The system is partitioned into simplexes using graph theory. A phase tree of the system has been designed, on the basis of which the number and compositions of phases crystallizing in stable elements have been predicted. A 3D model of the phase assemblage of the Ca,Ba‖F,Cl system has been designed in the KOMPAS 3D v21 software. The presence of a quasi-binary eutectic and the stability of the crystallizing phases (CaF_2 and $BaCl_2$) on the CaF_2–$BaCl_2$ stable diagonal were confirmed by thermogravimetry (TG) and X-ray powder diffraction (XRD).

Keywords: reciprocal system, eutectic, liquidus, thermogravimetry, X-ray powder diffraction, ion exchange reaction

DOI: 10.1134/S0036023623602556

INTRODUCTION

Phase diagrams of inorganic salt systems are of interest due to their wide application. Variations in the cationic and anionic compositions of salts offer a means to manufacture materials intended for solar batteries, phosphors, electrolytes, and for other functional purposes [1–7]. Eutectic salt mixtures are used as heat-storing materials [8]. Reciprocal salt pairs, of which ion-exchange reactions are typical, are valuable for progress in the theory of physicochemical analysis [9–12].

The three-component reciprocal system comprised of fluorides and chlorides of calcium and barium is a complex subject matter of study; its boundary binary systems have differing types of phase diagrams. Figure 1 images the development of the T–x–y diagram of the Ca,Ba‖F,Cl three-component reciprocal system, with the T–x diagrams of the boundary binaries adjoining to its lateral sides. In the CaF_2–$CaCl_2$ system, the incongruently melting compound CaFCl, a peritectic, and a eutectic are formed [13, 14] (Fig. 1). The $CaCl_2$–$BaCl_2$ system has the same type of phase diagram with the incongruently melting compound $CaBaCl_4$ [15]. The BaF_2–$BaCl_2$ system features the congruently melting compound BaFCl and two eutectics [13], and the CaF_2–BaF_2 system features a limited solid solution series with a minimum and peritectic equilibrium [17, 18] (Fig. 1). Thus, the boundary binary systems are represented by three different types of phase diagrams, which makes the Ca,Ba‖F,Cl subject matter an interesting model of phase equilibria and chemical interactions between components.

THEORETICAL ANALYSIS

Figure 2 shows the liquidus projection on the composition square of the Ca,Ba‖F,Cl three-component reciprocal system. All data on the constituent two-component systems and on invariant three-component compositions were analyzed while working with reference literature [15–17]. The binary compounds on the sides add secants and partition the ternary system into triangles. The partition into stable simplexes was carried out using graph theory [19]. The adjacency matrix for the vertices of the Ca,Ba‖F,Cl system was thus obtained (Table S1).

A logical expression was derived from the adjacency matrix, whose solution identified a set of unconnected graphs. By writing out the missing vertices, we obtained a set of stable simplexes:

$X_1X_3X_7$: CaF_2–BaF_2–BaF_2·$BaCl_2$;

$X_1X_4X_7$: CaF_2–$BaCl_2$–BaF_2·$BaCl_2$;

$X_1X_4X_5$: CaF_2–$BaCl_2$–CaF_2·$CaCl_2$;

$X_4X_5X_6$: $BaCl_2$–CaF_2·$CaCl_2$–$CaCl_2$·$BaCl_2$;

$X_2X_5X_6$: $CaCl_2$–CaF_2·$CaCl_2$–$CaCl_2$·$BaCl_2$.

Figure S1 images the phase tree of the Ca,Ba‖F,Cl system comprised of five stable triangles intercon-

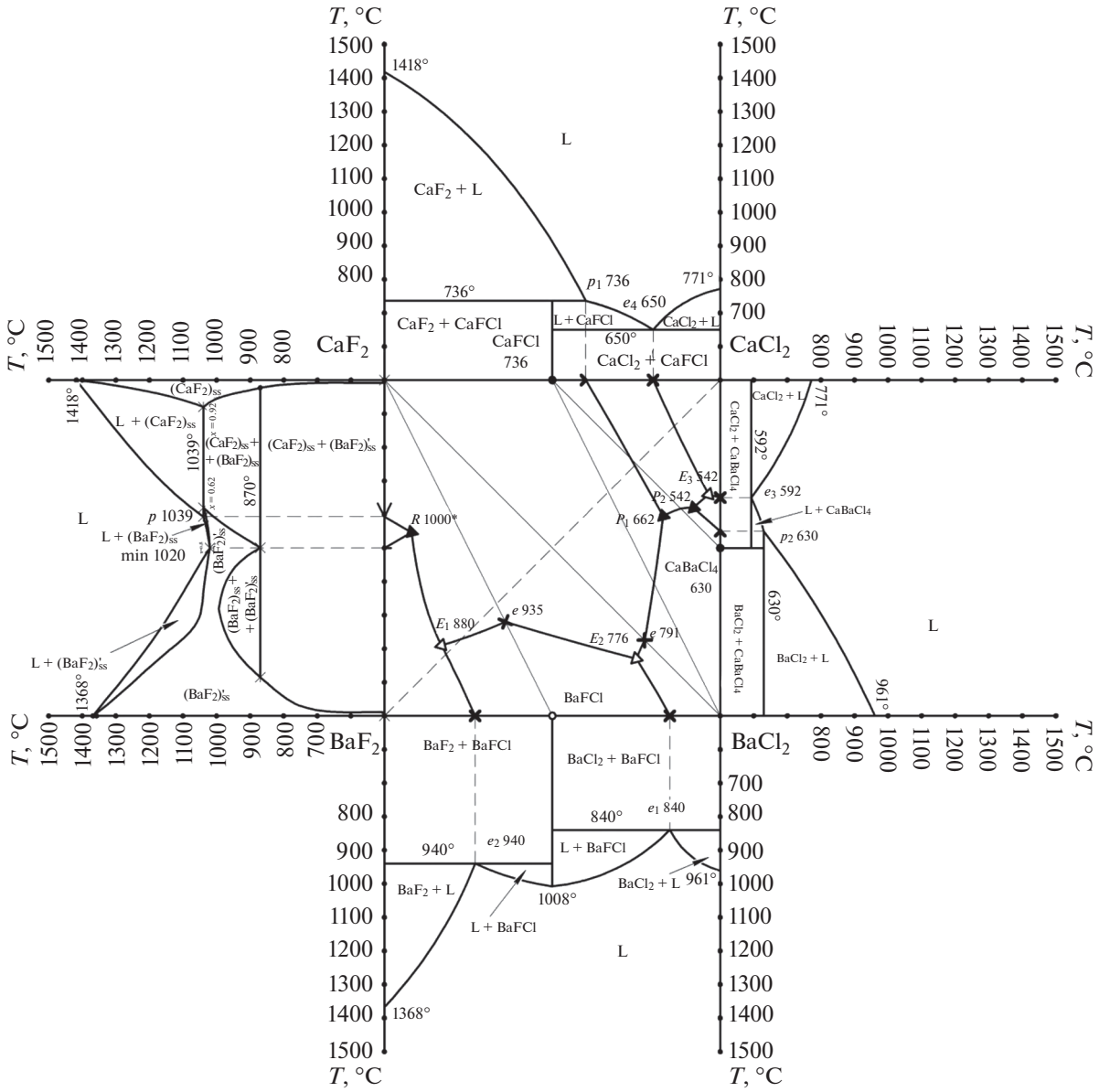

Fig. 1. Development of the *T*–*x*–*y* diagram of the Ca,Ba‖F,Cl ternary reciprocal system and *T*–*x* diagrams of the boundary binaries. *Predicted value.

nected by four stable secants. The phase tree is the basis for predicting phases that would crystallize; however, it is necessary to take into account the nature of interaction between the components, for example, the formation of congruent or incongruent compounds and areas of limited interstitial solid solutions.

In addition to the compounds formed on the binary sides (congruently melting BaFCl and incongruently melting $CaBaCl_4$ and CaFCl), the Ca,Ba‖F,Cl reciprocal system features 12 ion-exchange reactions at conversion points (denoted on Fig. S2). The reactions and the standard enthalpies and Gibbs free energies calculated for them can be found in the supplementary materials.

The reaction products are connected by solid lines on Fig. S2, and the starting products are connected by dashed lines. Therefore, the reaction products are the vertices of the stable elements of the phase tree (Fig. S1) and, accordingly, will crystallize from the melt.

3D-MODELING OF THE PHASE ASSEMBLAGE OF THE SYSTEM

A 3D model of the phase assemblage in the Ca,Ba‖F,Cl ternary reciprocal system was designed based on the experimentally determined melting temperatures of individual compounds, the compositions and melting temperatures at binary and ternary invari-

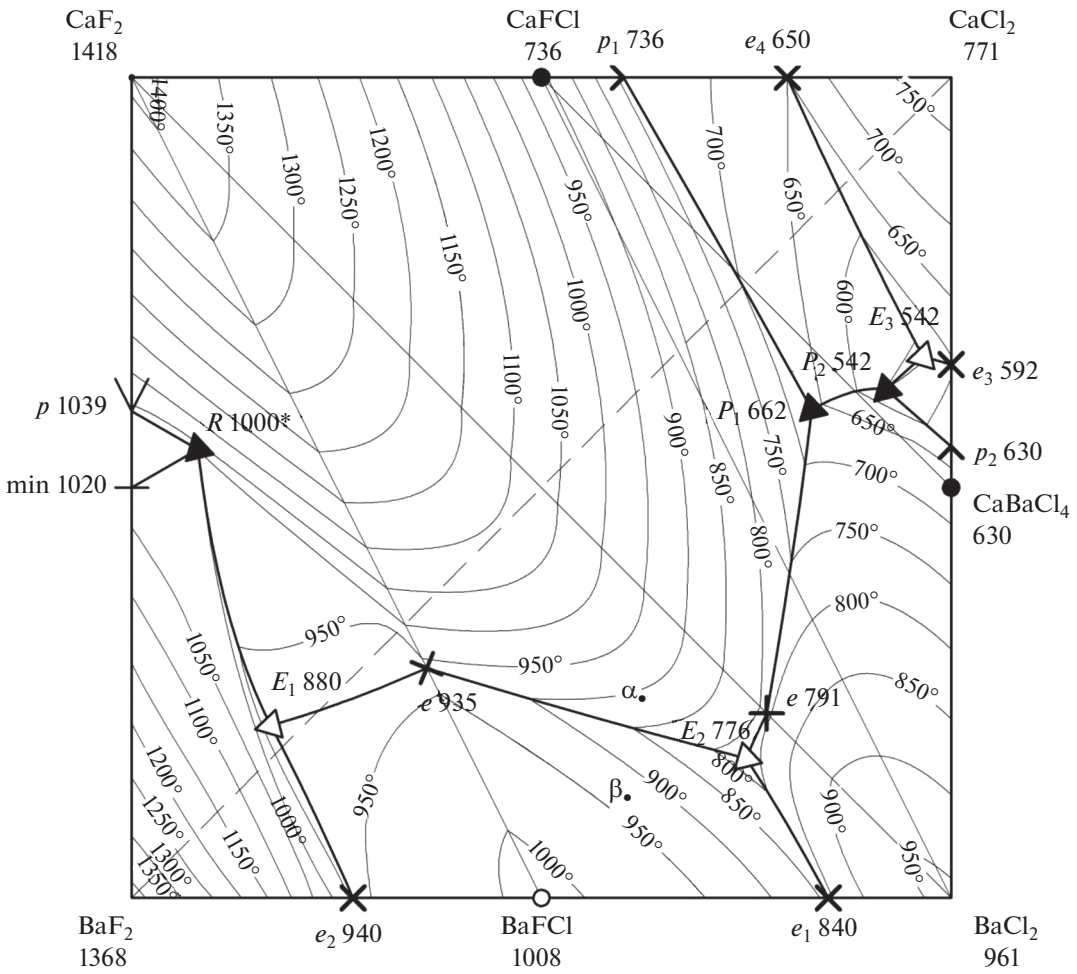

Fig. 2. Liquidus projection on the composition square of the Ca,Ba‖F,Cl ternary reciprocal system. * Predicted value.

ant points in the KOMPAS 3D v21 program [20, 21] in the (composition)–(phase transition temperature) space (Fig. 3). The base of the model is the composition square (in equiv. percent); the temperature is plotted along the vertical axis in the range of 500–1500°C [22].

EXPERIMENTAL

Experimental characterization of samples was carried out on an MOM Q-1500 derivatograph in the controlled heating mode from 25 to 1100°C at 20 K/min in platinum crucibles for a derivatograph with thermocouples attached to the bottom. The sample size was 1 g. All compositions are in equivalent fractions expressed as percent [23–26]. The chemicals used were specialty grade CaF_2, chemically pure grade BaF_2, chemically pure grade $BaCl_2$, and pure for analysis grade freshly calcined alumina used as the reference. The melting temperatures of the reagents corresponded to reference values [27]. X-ray powder diffraction (XRD) experiments were carried out on an Arl X'tra diffractometer using CuK_α radiation with a nickel β-filter.

RESULTS AND DISCUSSION

The liquidus surface isotherms of the system in 50°C steps (Fig. 2) were obtained based on the 3D model by intersecting the horizontal plane with the liquidus surface. Calcium fluoride has the largest crystallization field (Fig. 2). Since minimum point min 1020 and a peritectic point *p* 1039 occur on the CaF_2–BaF_2 side, the liquidus surface in the CaF_2–BaF_2–BaFCl simplex is predicted to feature wedging point *R* 1000*: $L + (BaF_2)_{ss} \rightleftarrows (CaF_2)_{ss} + (BaF_2)'_{ss}$, where $(BaF_2)_{ss}$ and $(BaF_2)'_{ss}$ are BaF_2-base limited solid solution phases, $(CaF_2)_{ss}$ is the CaF_2-base limited solid solution (Fig. 4), T=1000 and 900°C. Hereafter, ss stands for the solid solution. The degree of curvature of the liquidus surface can be judged from the density of isotherm arrangement.

The sections of the phase assemblage model at 1200, 1000, 900, and 700°C (Fig. 4) and at 800, 750, 650, and 600°C (Fig. 5) were obtained as intersections of a set applicate horizontal plane with surfaces of the model. The liquid area becomes smaller, and two-

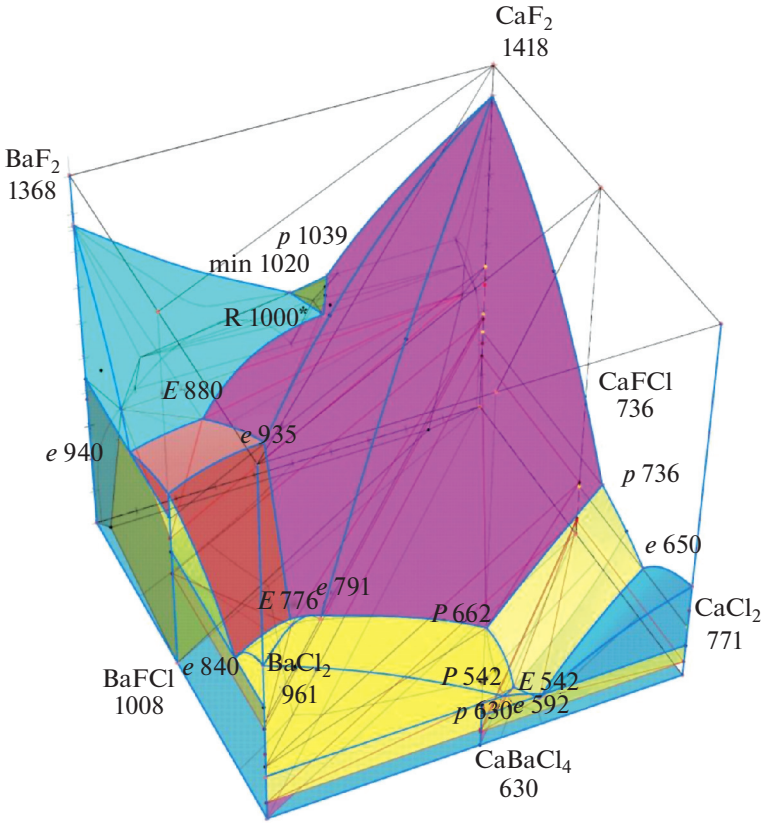

Fig. 3. 3D model of the phase assemblage of the Ca,Ba‖F,Cl system. *Predicted value.

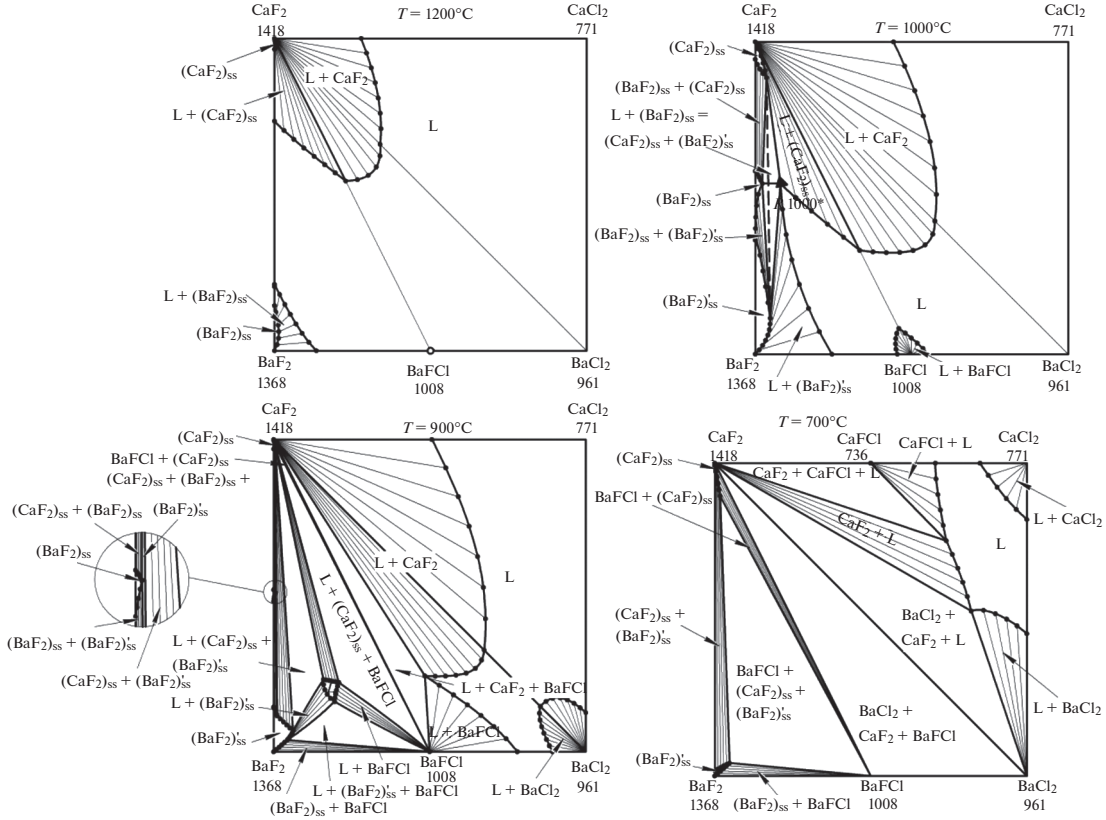

Fig. 4. 1200, 1000, 900, and 700°C isothermal sections of the Ca,Ba‖F,Cl system derived from the model.

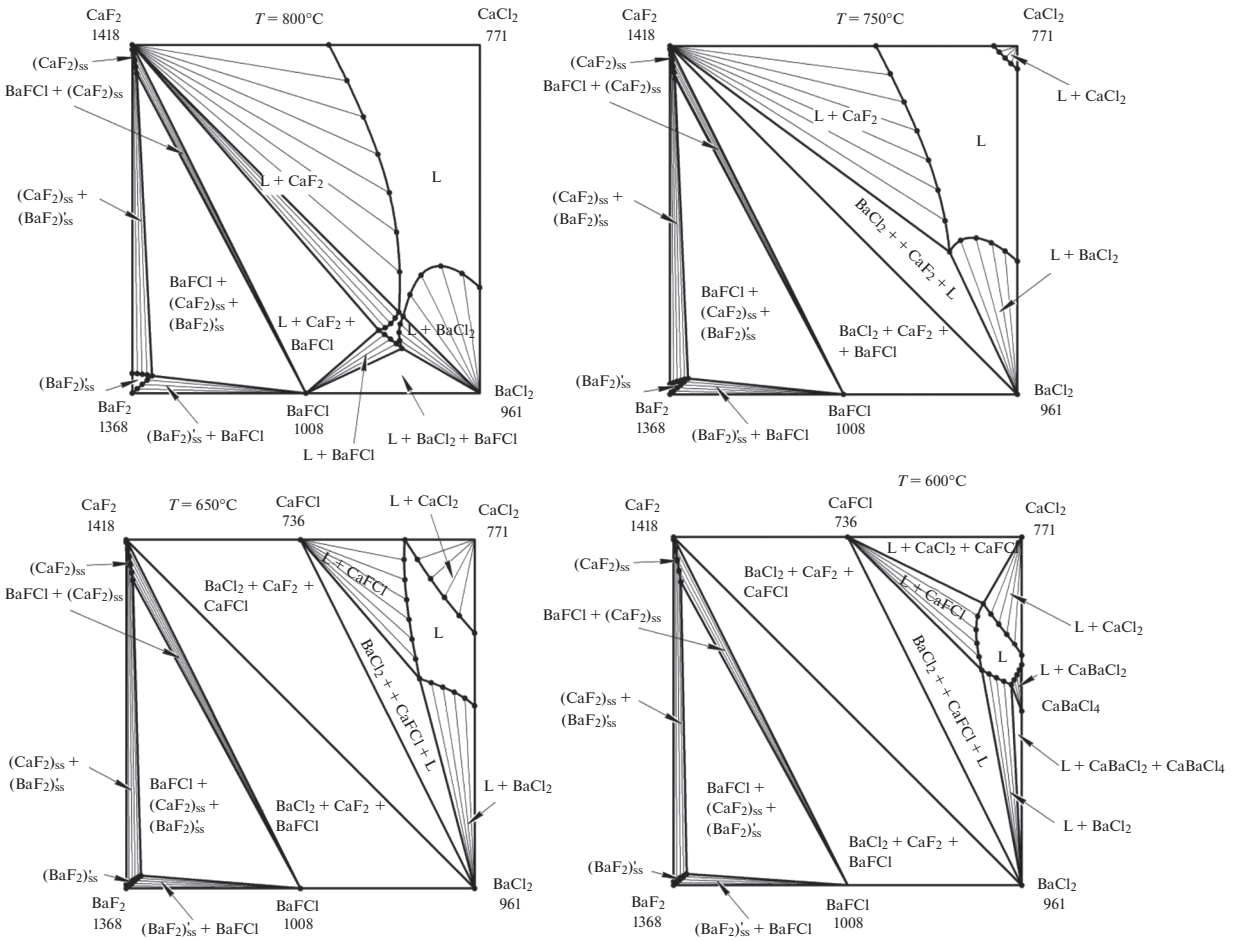

Fig. 5. 800, 750, 650, and 600°C isothermal sections of the Ca,Ba‖F,Cl system derived from the model.

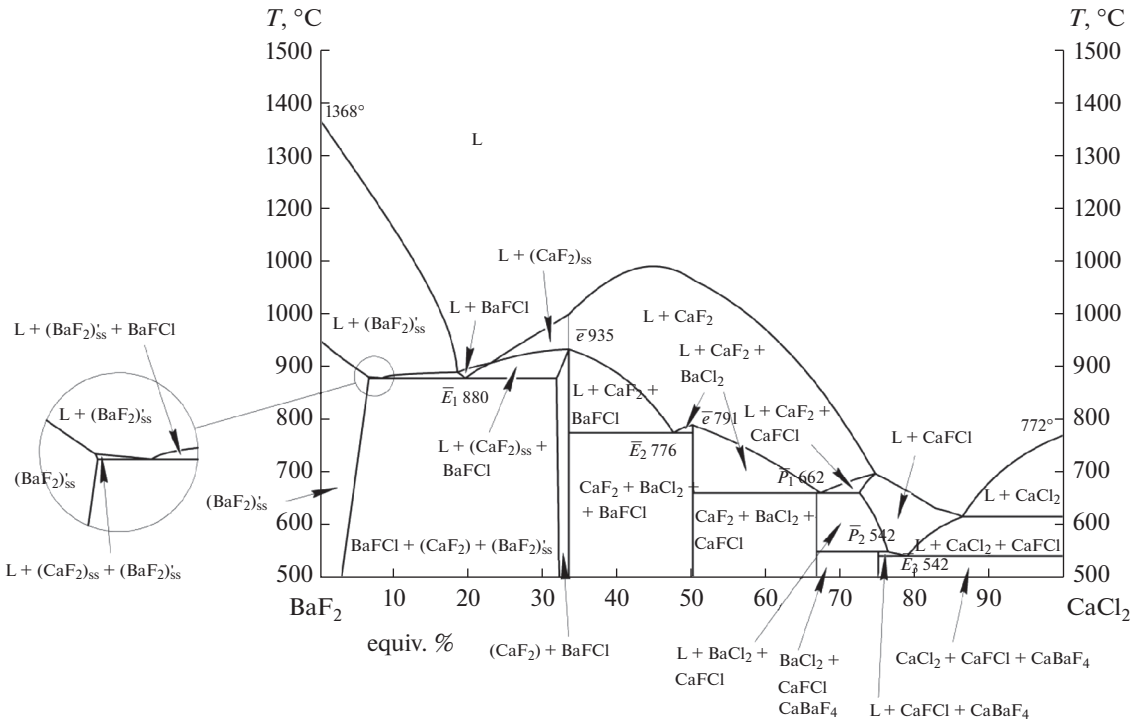

Fig. 6. Polythermal section of the BaF_2–$CaCl_2$ unstable diagonal of the Ca,Ba‖F,Cl system derived from the model.

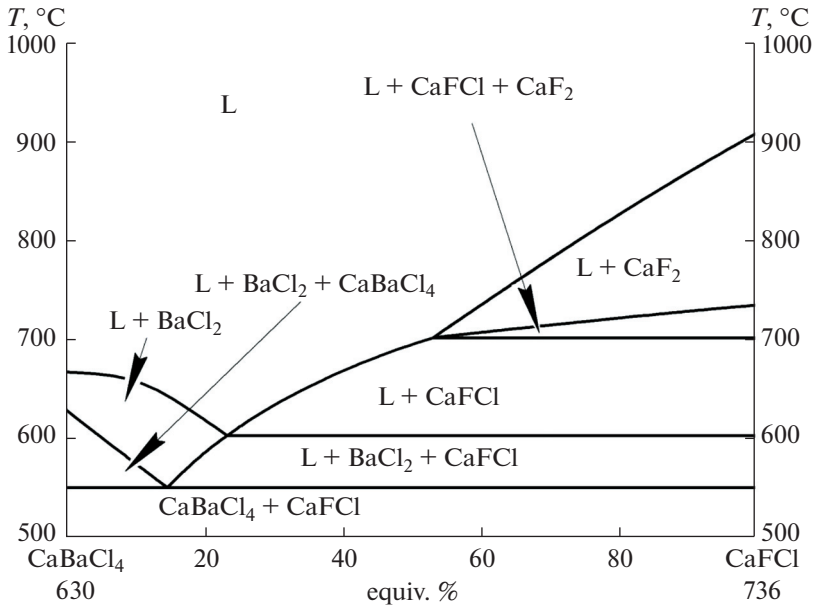

Fig. 7. Polythermal section of the $CaBaCl_4$–CaFCl secant of the Ca,Ba‖F,Cl system derived from the model.

phase and three-phase areas become larger, as temperature lowers. Polythermal sections of the BaF_2–$CaCl_2$ unstable diagonal and the $CaBaCl_4$–CaFCl secant were derived from the model (Figs. 6 and 7) via identifying the lines of intersection of the vertical plane with the surfaces of the figure. The $(BaF_2)_{ss}$ area is a BaF_2-base limited solid solution. The section features ray $\bar{E}_1880$ radiating from the BaFCl corner, rays $\bar{E}_2776$ and $\bar{P}_1662$ from the CaF_2 corner, and rays $\bar{E}_3542$ and $\bar{P}_2542$ from the CaFCl corner directed to invariant points: ternary eutectics E_1 880, E_2 776, and E_3 542; and ternary peritectics P_1 662 and P_2 542.

The phase-transformation temperatures upon crystallization were predicted for sample α (25% CaF_2, 15% BaF_2, 60% $BaCl_2$) and sample β (10% CaF_2, 30% BaF_2, 60% $BaCl_2$); the relevant figurative points appear in Fig. 2. Thermoanalytical (T, DTA, and curves TG) were also recorded for figurative points α and β (Figs. 6 and 7). Table 1 lists theoretical and experimentally measured values of these temperatures and phase transformation schemes. Relative deviations of the theoretical (predicted using the 3D model) and experimental temperatures were calculated using the relationship

$$\delta_i = \frac{\Delta T_i}{T_i^{\exp} + 273} \times 100\%,$$

where δ_i is the relative deviation of the experimental and theoretical values of temperature for the *i*th peak;

Table 1. Comparison of theoretically predicted and experimentally determined phase transformation parameters

Point	Phase-transition temperatures, °C		ΔT, K	δ, %	Phase reaction
	theoretical	experimental			
α	902	894	8	0.7	L = CaF_2
	835	790	45	4.2	L = CaF_2 + BaFCl
	776	776	0	0	L = CaF_2 + BaFCl + $BaCl_2$
β	948	952	4	0.3	L = BaFCl
	808	791	17	1.6	L = BaFCl + CaF_2
	776	776	0	0	L = CaF_2 + BaFCl + $BaCl_2$

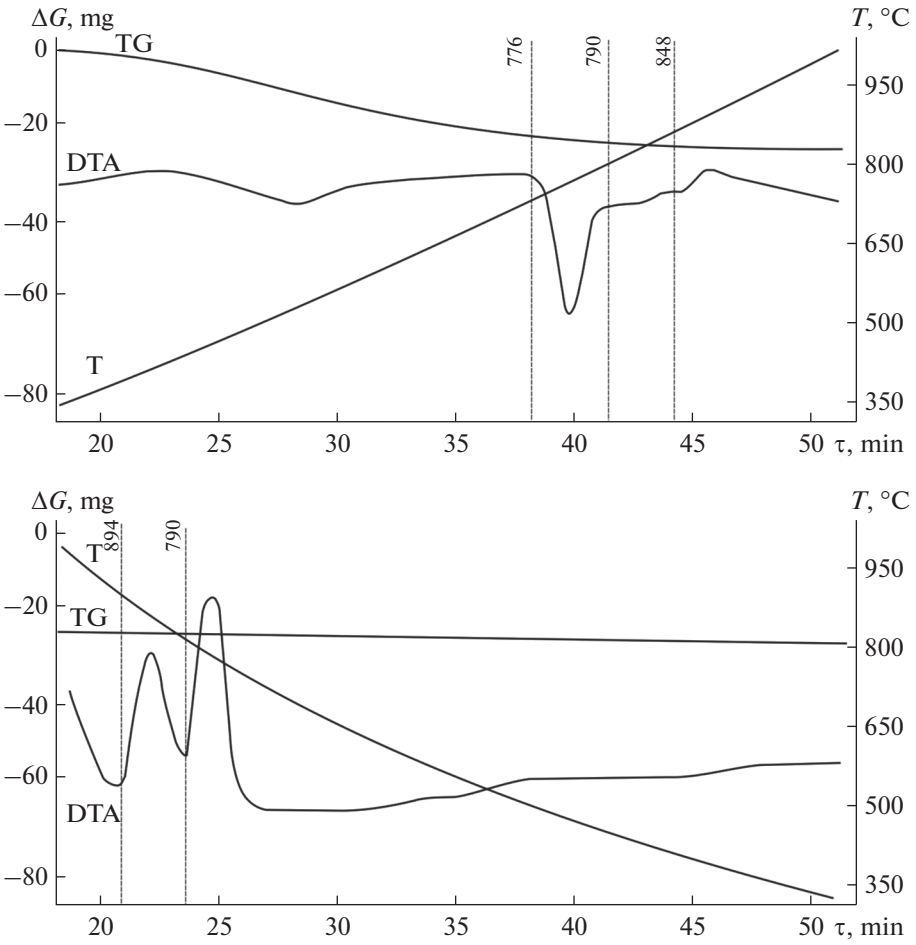

Fig. 8. Thermoanalytical heating and cooling curves for sample α (25% CaF_2, 15% BaF_2, 60% $BaCl_2$).

T_i^{exp} is the experimentally measured temperature in the *i*th peak; $\Delta T_i = \left|T_i^{exp} - T_i^{theor}\right|$ is the absolute deviation of the experimental and theoretical T_i^{theor} values of temperature for the *i*th peak.

The δ values in Table 1 indicate a good convergence of results and the adequacy of prediction of phase-transformation temperatures in three-component reciprocal systems by means of 3D phase diagram models.

In order to confirm the occurrence of reaction at conversion point *K* (Fig. S2) and the stability of the salt pair, we performed thermal analysis of a 22.5% CaF_2 + 77.5% $BaCl_2$ sample, which was previously assigned to a quasi-binary eutectic [15]. Our results differed slightly from the previously published data [15]. The DTA curve featured two events (at 881 and 793°C); therefore, the composition did not correspond to a eutectic alloy (Figs. 8 and 9). The sample was then removed from the crucible and subjected to X-ray powder diffraction analysis, the results of which are shown in Fig. 10.

CONCLUSIONS

The thermoanalytical curves for a 22.5% CaF_2 + 77.5% $BaCl_2$ sample and XRD data (Fig. 8) imply that the CaF_2–$BaCl_2$ diagonal is a stable diagonal; that is, for the reaction at point *K* this salt pair is the product of the reaction $CaCl_2 + BaF_2 \rightleftarrows CaF_2 + BaCl_2$. Therefore, the diagonal partition has been verified for the Ca,Ba‖F,Cl ternary reciprocal system. The secant lines connected by vertices to the central diagonal are stable: CaF_2–BaFCl, $BaCl_2$–CaFCl (Fig. S2). The spatial model of the Ca,Ba‖F,Cl phase diagram visually represents the phase assemblage as a set of spaces of phase states, i.e., phase areas. Each area describes certain phase equilibrium in the system and is separated from other areas by interfaces.

SUPPLEMENTARY INFORMATION

Online version contains supplementary materials available at https://doi.org/10.1134/S0036023623602556.

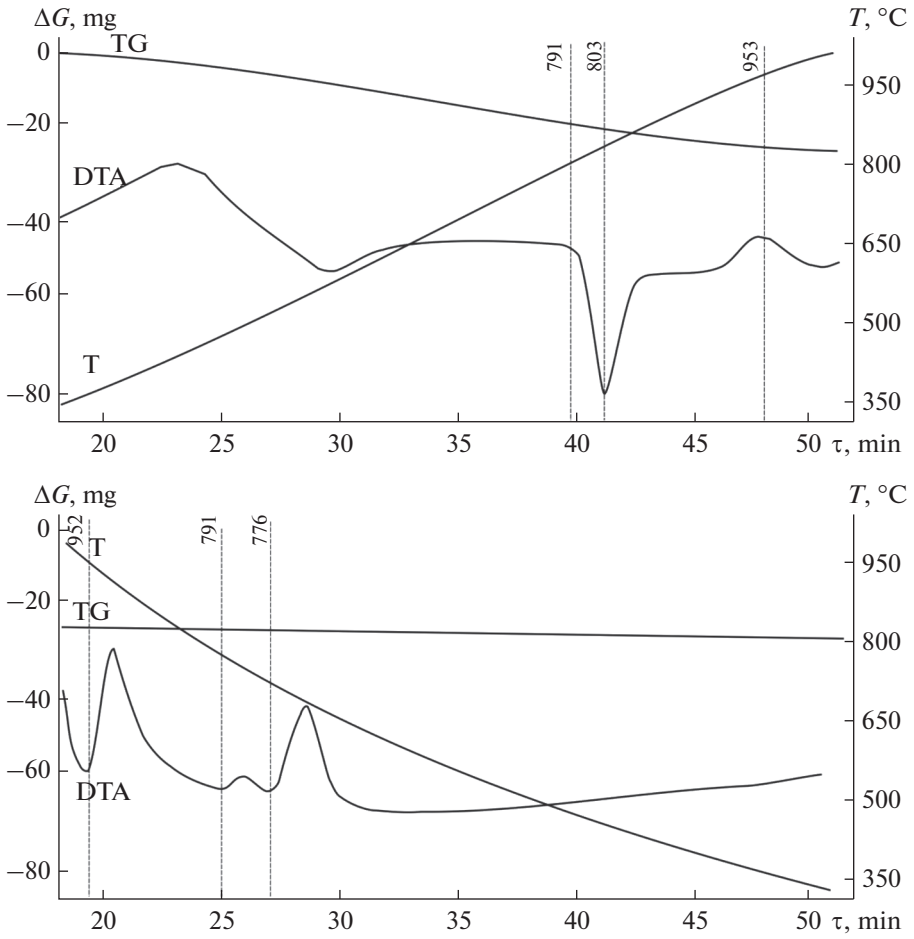

Fig. 9. Thermoanalytical heating and cooling curves for sample β (10% CaF_2, 30% BaF_2, and 60% $BaCl_2$).

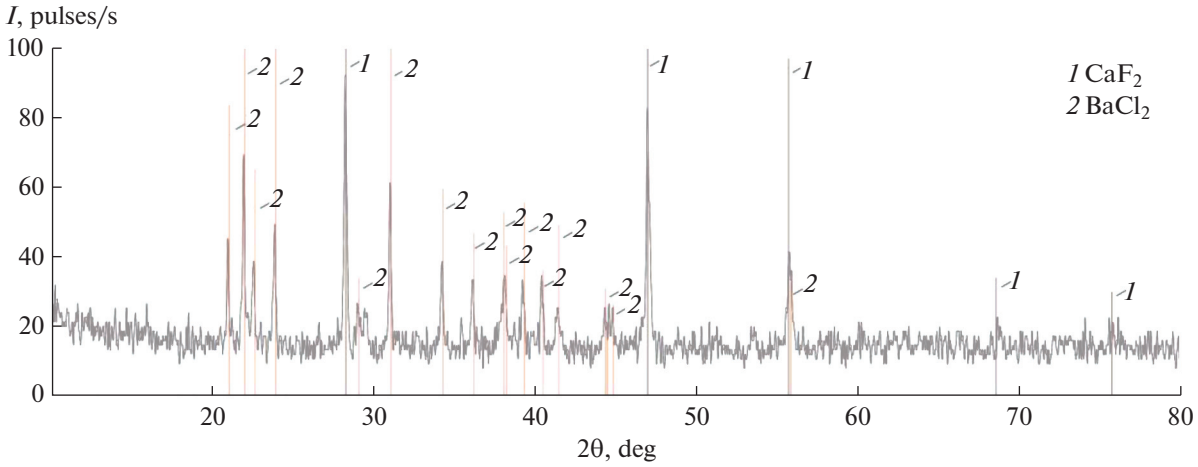

Fig. 10. X-ray diffraction pattern of a 22.5% CaF_2 + 77.5% $BaCl_2$ sample (CaF_2: PDF 00002-1302; $BaCl_2$: PDF 01-072-0368).

FUNDING

The work was supported by the Ministry of Science and Higher Education of the Russian Federation (theme No. FSSE-2023-0003) as part of the Government assignment to Samara State Technical University.

CONFLICT OF INTEREST

The authors declare that they have no conflicts of interest.

REFERENCES

1. D. Sveinbjörnsson, A. S. Christiansen, R. Viskinde, et al., J. Electrochem. Soc. **161**, A1432 (2014). https://doi.org/10.1149/2.1061409jes
2. R. Semwal, C. Ravi, R. Kumar, et al., Org. Chem. **84**, 792 (2019). https://doi.org/10.1021/acs.joc.8b02637
3. Q. Gong, W. Ding, A. Bonk, et al., J. Power Sources **475**, 228674 (2020). https://doi.org/10.1016/j.jpowsour.2020.228674
4. S. S. Abdullaeva, F. M. Mammadov, and I. B. Bakhtiyarly, Russ. J. Inorg. Chem. **65**, 100 (2020). https://doi.org/10.1134/S0036023619110020
5. U. A. Gasanova, O. M. Aliev, I. B. Bakhtiyarly, et al., Russ. J. Inorg. Chem. **64**, 242 (2019). https://doi.org/10.1134/S0036023619020074
6. S. K. Jahangirova, S. H. Mammadov, D. S. Ajdarova, et al., Russ. J. Inorg. Chem. **64**, 1169 (2019). https://doi.org/10.1134/S0036023619090092
7. I. Nizomov and L. Soliev, Russ. J. Inorg. Chem. **64**, 531 (2019). https://doi.org/10.1134/S0036023619030148
8. B. D. Babaev, High Temperature **52**, 736 (2014). https://doi.org/10.1134/S0018151X14050010
9. I. Rychlowska–Himmel and M. Bosacka, Thermochim. Acta **503–504**, 1325 (2010). https://doi.org/10.1016/j.tca.2010.03.002
10. P. Haseli, R. Jacob, and M. Liu, Thermochim. Acta **695**, 178811 (2021). https://doi.org/10.1016/j.tca.2020.178811
11. N. A. Kozyreva and E. S. Gryzlova, Russ. J. Inorg. Chem. **54**, 772 (2009).
12. O. S. Kudryashova, A. M. Elokhov, E. E. Garbuz, et al., Russ. J. Inorg. Chem. **65**, 1905 (2020). https://doi.org/10.1134/S0036023620120104
13. V. I. Posypaiko and E. A. Alekseeva, *Fusibility Diagrams for Salt Systems*, part III (Metallurgiya, Moscow, 1979) [in Russian].
14. D. A. Wenz, I. Johnson, and R. D. Wolson, J. Chem. Eng. Data **14**, 250 (1969). https://doi.org/10.1021/je60041a027
15. N. K. Voskresenskaya, N. N. Evseeva, S. I. Berul', et al., *Handbook of Fusibility of Anhydrous Inorganic Salt Systems*, vol. 2 (Izd. AN SSSR, Moscow, 1961) [in Russian].
16. G. A. Bukhalova and A. G. Bergman, Zh. Obshch. Khim. **21**, 1570 (1951).
17. P. P. Fedorov, I. I. Buchinskaya, N. A. Ivanovskaya, et al., Dokl. AN **401**, 652 (2005).
18. A. Düvel, P. Heitjans, P. P. Fedorov, et al., Solid State Sci. **83**, 188 (2018). https://doi.org/10.1016/j.solidstatesciences.2018.05.011
19. O. Ore, *Graph Theory* (Nauka, Moscow, 1980) [in Russian].
20. N. B. Ganin, *Design and Strength Calculations in the System KOMIIAC-3D V13* (DMK Press, Moscow, 2011) [in Russian].
21. OOO "ASKON—Design systems." https://kompas.ru/ (dated October 27, 2022).
22. A. V. Burchakov, I. K. Garkushin, I. M. Kondratyuk, et al., Russ. J. Inorg. Chem. **66**, 1021 (2021). https://doi.org/10.1134/S0036023621070044
23. V. P. Egunov, *Introduction to Thermal Analysis* (Samara, 1996) [in Russian].
24. M. Wagner, *Thermal Analysis in Practice: Fundamental Aspects* (Hanser Publications, 2018).
25. Yu. V. Moshchenskii, Prib. Tekh. Eksper. **46**, 143 (2003).
26. S. V. Fedotov and Yu. V. Moshchenskii, *Interface Software DSCTool* (Samar. Gos. Tekhn. Univ., Samara, 2004) [in Russian].
27. *Thermal Constants of Substances*: A Handbook, Ed. by V. P. Glushko (VINITI, Moscow, 1981) [in Russian].

Translated by O. Fedorova